ARTICLE

Context Dependence of the Assembly, Structure, and Stability of Polypeptide Multilayer Nanofilms

Ling Zhang,[†] Wanhua Zhao,[†] Jai S. Rudra,[‡] and Donald T. Haynie[†,‡,*]

[†]Artificial Cell Technologies, Inc., 5 Science Park at Yale, Third Floor, New Haven, Connecticut 06511, [‡]Bionanosystems Engineering Laboratory, National Dendrimer and Nanotechnology Center, and Department of Chemistry, College of Science & Technology, Central Michigan University, Mount Pleasant, Michigan 48859

ABSTRACT Polyelectrolyte multilayer nanofilms and nanocomposites have shown considerable promise for the rational development of multifunctional materials with wide-ranging properties. Polypeptides are a distinctive and largely unexplored class of polyelectrolytes in this context. Methods now exist for the synthesis of peptides with control at the level of the amino acid sequence, and for the preparation of these polymers in massive quantities. Here, we analyze the roles of six designed 32mer peptides in the fabrication, structure, and stability of multilayer nanofilms prepared by layer-by-layer self-assembly. The data show that amino acid sequence and the specific combination of anionic and cationic peptides together have a marked impact on nanofilm growth behavior, secondary structure content, and density in experimental studies. The same factors determine physical properties of the corresponding interpolypeptide complexes in molecular dynamics simulations.

KEYWORDS: layer-by-layer assembly · molecular dynamics multilayer film · noncovalent interaction · peptide

Preparation of polyelectrolyte multilayer films by layer-by-layer assembly (LBL)[1] is attractive for a host of reasons. For example, polymers can be deposited inexpensively from aqueous solution onto a solid support, minimizing the involvement of organic solvents; the process itself is environmentally benign. Moreover, the films can be built on substrates of virtually any size or shape, and the layering process can be automated, which is important for industrialization. Furthermore, diverse linear ionic polymers and natural biomacromolecules are demonstrably suitable for fabrication of multilayer films,[1–4] including polypeptides.[5] The general approach therefore holds promise for the development of novel materials which have realistic prospects for large-scale production and commercialization.

In ordinary polyelectrolyte LBL, strong electrostatic interactions both limit the amount of material deposited per layer and stabilize the multilayer film structure.[1,6] Hydrophobic interactions and hydrogen bonding too can influence polymer assembly and the properties of the resulting films.[7–9] Less clear is how the various kinds of noncovalent interactions will influence film assembly, stability, and other physical properties in any particular polyelectrolyte system. Increased knowledge of the roles of noncovalent interactions will be important for the full exploitation of polypeptide films in practical applications.[10]

Polypeptides are unique among organic polymers in being able to form the familiar secondary, tertiary, and quaternary structures displayed by folded proteins.[11,12] Control of peptide adsorption properties, through control of peptide structure or assembly conditions, translates into control of the physical, chemical, and biological properties of the polypeptide multilayer nanofilms.[5,10] Experimental studies have shown that dried polypeptide multilayer nanofilms resemble folded globular proteins in being crystal-like.[13] In addition, both proteins and polypeptide multiayer nanofilms are stabilized by noncovalent interactions,[5] and both generally feature a substantial proportion of amino acid residues in their secondary structure.[13–16] Reversible formation of disulfide bonds between cysteine-containing peptides increases nanofilm stability at neutral pH and in harsh environments,[10,15–19] mimicking the well-known stabilization of the native structure of disulfide bond-containing hormones and proteins,[11] and enabling control over film properties by changing the reducing potential.[5,19,20]

Complementary approaches have provided insight on causal relationships pertaining to polyelectrolyte multilayer film structure and function. For instance, the results of molecular dynamics (MD) studies of model polypeptide multilayer nanofilms are consistent with the view that electrostatic interactions, hydrophobic interac

*Address correspondence to haynie@jhu.edu.

Received for review September 30, 2007 and accepted November 05, 2007.

Published online December 8, 2007.
10.1021/nn700267g CCC: $37.00

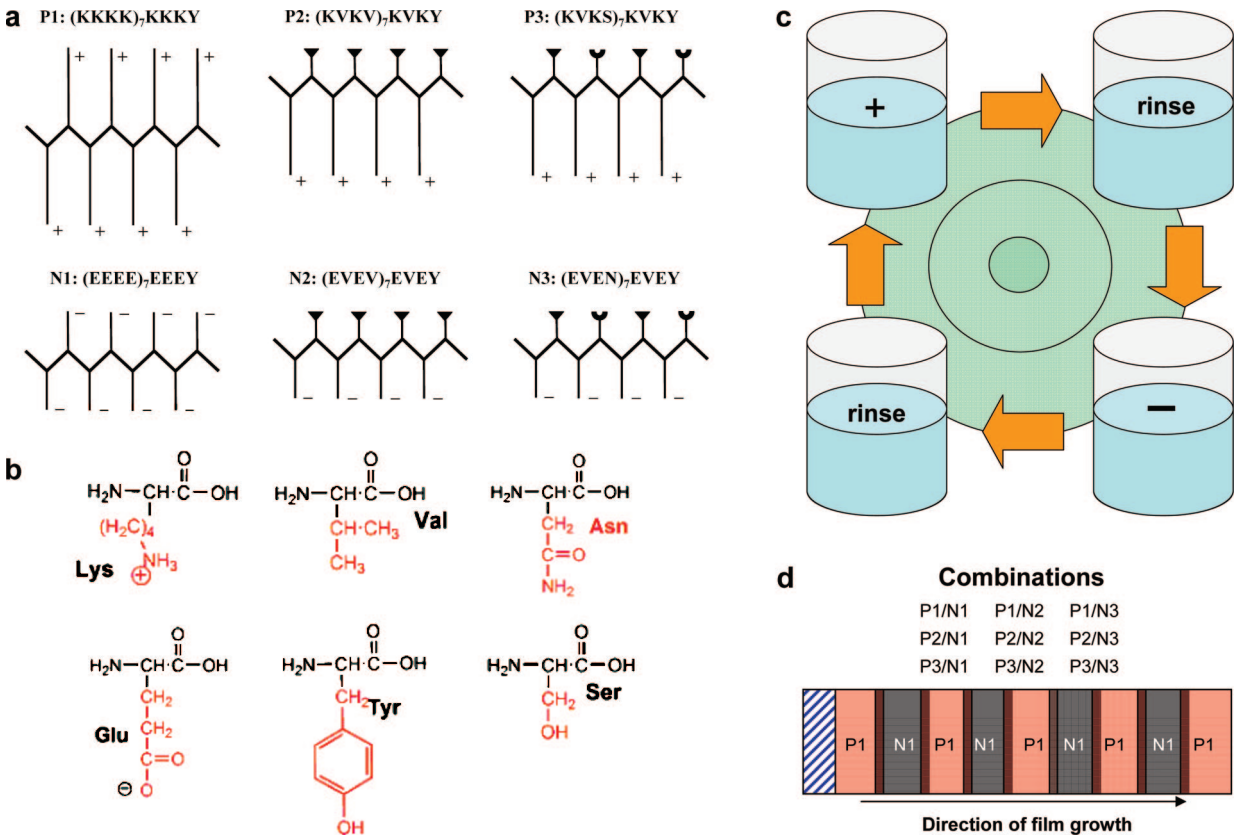

Figure 1. Polymer structure and assembly method. (a) Schematic diagrams of the designed 32mer peptides at neutral pH. The single-letter code is used to indicate peptide structure: K, lysine; E, glutamic acid; V, valine; S, serine; N, glutamine. Tyrosine, Y, was included for quantification of concentration by aromatic absorbance at 280 nm. All peptides are shown in β sheet conformation (cf. Figure 2a and Table 2): alternating side chains point above and below the plane of the sheet, which is perpendicular to the plane of the page. Side-chain lengths and physical properties vary from peptide to peptide. P1 and N1 were designed to probe the role of electrostatic interactions in multilayer film assembly; P2 and N2, hydrophobic interactions; P3 and N3, side-chain hydrogen bonding. (b) Side chains of the amino acids used to synthesize the peptides depicted in panel a. Lys and Glu are ionized at neutral pH. Val is always hydrophobic. Ser and Asn are polar but not ionized. (c) Layer-by-layer assembly. Polypeptide multilayer films were prepared by sequential deposition of polycationic peptides and polyanionic peptides on a solid support from aqueous solution at neutral pH. Under such conditions, the linear charge density of the polymers is high. Films were rinsed between polymer adsorption steps to remove loosely bound material and dried to minimize the water content for characterization. (d) Multilayer films studied here. The substrate is shown at the left. Film growth proceeds to the right. Layers of P1 and of N1 are deposited in successive polymer adsorption steps. There is some overlap of material in adjacent layers. Nine combinations of designed peptide have been studied in this research.

-tions, and hydrogen bonds influence peptide self-assembly in a multilayer film context.[21] Physical properties of interpolyelectrolyte complexes (IPECs) of various combinations of polyelectrolytes have been investigated extensively;[22] soluble IPECs are now considered key conceptual antecedents of polyelectrolyte multilayer films, which are a sort of condensed phase of highly aggregated IPECs. Nevertheless, many questions remain concerning the physics of polypeptide self-assembly in multilayer nanofilms.[10] Answering such questions will increase the predictability of the polypeptide multilayer nanofilm fabrication process and promote an understanding of the nature of matter in the transition from molecules to aggregates of molecules to bulk material.

Here, polypeptide multilayer film assembly, surface morphology, internal structure, and structural stability and the structure and energetics of polypeptide complexation have been studied for different systems of cationic 32mers and anionic 32mers.

RESULTS AND DISCUSSION

Six peptide structures have been designed, synthesized, and purified in order to study the role of different kinds of noncovalent interactions in multilayer nanofilm formation and stability (Figure 1a). P1 and N1 represent electrostatic interactions; P2 and N2, hydrophobic interactions; and P3 and N3, side-chain hydrogen bonding.[23] Figure 1b depicts the side chains of these polymers. The Lys side chain is positively charged, whereas that of Glu is negatively charged at neutral pH. There are twice as many methylene groups in Lys as in Glu. Val has a purely hydrophobic side chain. The hydroxyl group of Ser is a hydrogen bond donor; the side chain of Asn can be a hydrogen bond acceptor or donor. The aromatic ring of Tyr is useful for spectroscopic detection. At pH 7.4, the absolute linear charge density $\lambda \approx 1$ per amino acid residue for P1 and N1; $\lambda \approx 0.5$ for P2, N2, P3, and N3.[11,24] As to hydrophobicity, (P2 or N2) > (P3 or N3) > (P1 or N1).[25] Control over amino acid sequence thus allows control over the abil-

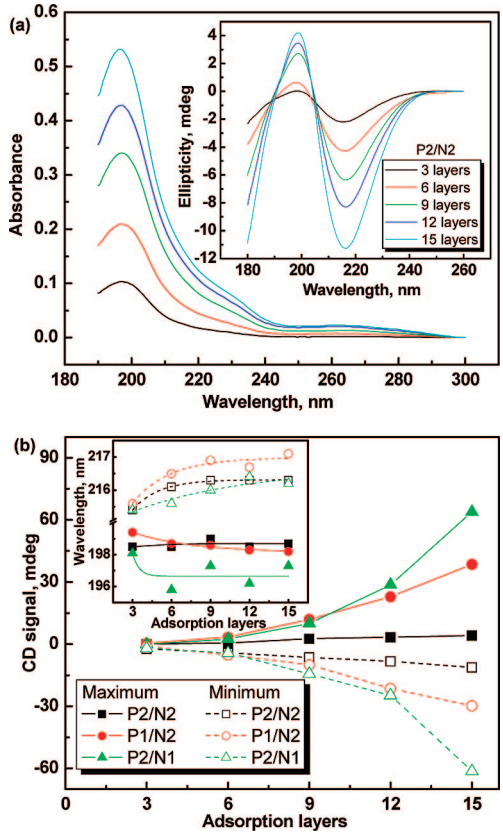

Figure 2. Fabrication of P2/N2, P1/N2, and P2/N1, monitored by optical spectroscopy. (a) UV spectra of P2/N2. Inset, CD spectra of P2/N2. (b) Magnitude of positive CD absorption bands at 198 nm (filled symbols) and negative absorption bands at 216 nm (open symbols) in millidegrees. The behavior in each case is corroborated by QCM measurements. Inset, location of peak maximum in nanometers. The shift in spectral properties indicates a dependence of internal film structure on thickness; the dependence varies with peptide system.

ity of peptides to form different noncovalent interactions. The relatively high value of λ enables controlled incorporation of peptides into multilayer films.[1,26]

Ionized amino acid side chains are generally found on the surface in folded proteins, where the charged groups determine aqueous solubility and binding specificity.[11] The hydrophobic "force", which drives nonpolar side chains to associate in a polar solvent, is generally considered to be the dominant force in protein folding; the "core" of a folded protein is predominantly hydrophobic.[27,28] Backbone hydrogen bonds stabilize secondary structures, α helices, and β sheets;[12] side-chain hydrogen bonds stabilize tertiary structure, whether the hydrogen bond is formed with another side chain or with the polypeptide backbone.

Conventional polyelectrolytes, for instance poly(styrene sulfonate) and poly(allylamine), are nonchiral; they do not form regular structure under typical conditions. Polypeptides, which are chiral, therefore present advantages for analyzing the internal structure of nanofilms. Circular dichroism spectrometry (CD) measures the difference in absorption between right- and left-circularly polarized light. The far-UV CD signal is remarkably sensitive to the conformation of the polypeptide backbone,[12] whether the peptides are in solution [29–31] or in a film.[32,33]

The nine oppositely charged combinations of the polypeptide designs in Figure 1a are indicated in Figure 1d. All nine combinations have been analyzed here, experimentally in a multilayer film context by CD, ultraviolet spectroscopy (UVS), and quartz crystal microbalance (QCM), and computationally in an IPEC context by MD simulations in implicit solvent. Nanofilm density has been found to vary by well over an order of magnitude, depending on the peptide system, and experimental film surface roughness has been found to correlate with the calculated potential energy of the corresponding IPEC. The results provide clues as to how peptide primary structure will determine self-assembly behavior and physical properties of multilayer films. These general conclusions are based on the following data.

Experiments. Multilayer nanofilm fabrication of all oppositely charged combinations of P1, N1, P2, and N2 has been characterized by UVS, CD, and QCM. Figure 2a shows spectra of the P2/N2 system at different stages of nanofilm fabrication. A substantial increase in optical density results from the deposition of each layer of polypeptide, indicating successive increases in nanofilm thickness. Film growth is an approximately linear function of the number of polymer adsorption steps in the range shown.

Structural changes within P2/N2 during the assembly process are apparently "cooperative", judging by the coincidence of signal intensity at specific wavelengths (~190 and ~205 nm). That is, the adsorption process seems not to involve reorganization of peptide structure during nanofilm buildup; if structure reorganization did occur, the variation in CD signal intensity would be a function of wavelength. The P1/N2 system, by contrast, shows supralinear growth (Figure 2b), whereas for P2/N1 growth is exponential and for P3/N2 it is non-cooperative (see Supporting Information).

The collective spectroscopic data support the view that the self-assembly of a given polypeptide design, *e.g.*, P2, during multilayer nanofilm fabrication is "context dependent". In other words, the assembly behavior of a given peptide molecule is determined as much by its own structure as by that of its oppositely charged assembly partner. Film mass for a fixed number of layers corroborates the general conclusion of context dependence (Figure 2b and Table 1). This perspective gains yet further support from the observation that the positive (198 nm) and negative (216 nm) CD band amplitudes are generally consistent with the corresponding UVS amplitudes and QCM mass increments (Table 1).

The context dependence of peptide behavior in nanofilm fabrication and structure resembles the "con-

TABLE 1. Physical Properties of Dry Polypeptide Multilayer Nanofilms[a]

film structure	frequency shift (Hz)	absorbance	thickness (nm)	granule size (nm)	growth mode
P1/N1	800	0.02	4.4	46	L
P1/N2	4700	1.40	43.9	204	S
P1/N3	1500	0.09	3.5	104	L
P2/N1	6600	2.77	72.8	86	S
P2/N2	1500	0.53	49.9	95	L
P2/N3	4300	0.60	46.3	150	S
P3/N1	1400	0.13	14.6	75	L
P3/N2	1000	0.40	31.3	160	L
P3/N3	500	0.15	11.5	140	L

[a]Frequency shift after 16 layers, measured by QCM, is proportional to actual mass deposited; UVS absorbance after 15 layers is a measure of optical thickness; ellipsometric thickness was determined after 20 layers; granule size after deposition of 20 layers was determined by AFM (see Figure 4). Apparent growth mode: S, supralinear; L, linear. The experimental thickness of a single layer of P1/N1 is 0.22 nm. For comparison, the dimensions of a 32mer peptide in extended conformation are roughly 10.5 nm × 1.5 nm × 0.5 nm. This implies uncertainty in the ellipsometric thickness or incomplete surface coverage during initial adsorption steps, especially when λ is high. Ellipsometric thickness is a fitting parameter, as is index of refraction. It must nevertheless be assumed that the measured values indicate relative film thickness and moreover approximate actual thickness.

TABLE 2. Results of Deconvolution of CD Spectra after Deposition of 15 Layers[a]

	secondary structure content			
film structure	α helix	β sheet	β turn	random coil
P1/N1	–	–	–	–
P1/N2	0	0.72	0.04	0.24
P1/N3	0.08	0.41	0.21	0.31
P2/N1	0	0.92	0.05	0.03
P2/N2	0	0.19	0.12	0.70
P2/N3	0	0.24	0.19	0.57
P3/N1	0.09	0.35	0.24	0.32
P3/N2	0	0.26	0.23	0.51
P3/N3	0.07	0.37	0.22	0.34

[a]β sheet, β turn, and random coil are prevalent in all the nanofilms; little α helix is present in any of them. P1/N2, P2/N1, P1/N3, and P3/N1 ("mismatched" combinations involving P1 or N1) have a large amount of β sheet, whereas P2/N2, P2/N3, P3/N2, and P3/N3 ("matched" combinations) have a large amount of random coil. MD simulations have revealed that the conformation of the corresponding IPECs is "extended" in the "mismatched" combinations and "bent" or "collapsed" in the "matched" ones (excluding P1/N1).

formation switching" exhibited by some peptides and proteins,[34] the context dependence of β sheet propensities,[35] and the context dependence of contributions of backbone hydrogen bonds to β sheet folding energetics.[36] The rules whereby a disordered polypeptide chain folds spontaneously into a functional small globular protein cannot be fundamentally different from the rules governing the organization of matter in a polypeptide multilayer nanofilm.

Closer analysis of the CD spectra of 15-layer films has revealed additional dissimilarities in structure between nanofilms which have just one polypeptide structure in common. The amplitude of the negative absorption band in the P2/N2 spectrum, for example, is about 2.7 times the size of the positive band (Figure 2a), the positive band is a factor of 1.3 greater than the amplitude of the negative one in the P1/N2 spectrum, and in the P2/N1 spectrum the two bands have about the same amplitude (Figure 2b). The differences in relative band amplitude suggest differences in film structure. The signal-to-noise ratio of the P1/N1 system is poor; these films are very thin under the conditions of the experiments reported here. P1/N1 nanofilms made of a greater number of layers do show a significant CD signal, as do 15-layer films of high-molecular-weight poly(L-lysine) and poly(L-glutamic acid).[1,37]

Shifts in position of the positive and negative CD absorption peaks during film fabrication have been found to resemble peak amplitude changes for all combinations of peptides. The positive band is blue-shifted on film buildup, whereas the negative band shifts to the red (inset, Figure 2b). In the P2/N2 system, the positive adsorption band shifts initially to the red and then to the blue by as much as 0.5 nm; the negative band shifts 0.9 nm to the red. The negative band of P1/N2 shifts to the red over 50% more than this, with further change probable on increasing the number of layers. The oscillatory behavior of the positive band of P2/N1 with successive peptide adsorption steps, which are as large as 2.3 nm peak-to-peak, suggests that nanofilm surface charge, or the migration of polymers within the film during the adsorption process, influences internal film structure.

The CD spectra of dried polypeptide nanofilms (*e.g.*, inset of Figure 2a) closely resemble the spectra of model β sheets in aqueous solution.[30,38] This alone strongly suggests that the peptides of the present study adopt a β sheet conformation on incorporation into a multilayer film. Deconvolution aims at the accurate resolution of a CD spectrum into contributions from a small number of more elementary structures, typically α helix, β sheet, β turn, and random coil.[39] The deconvoluted secondary structure content of the present nanofilms (Table 2) suggests that little if any α helix is present in the 15-layer structures at neutral pH (or in any of the uncomplexed peptides in solution, data not shown; helical structure can be formed in a polypeptide multilayer nanofilm at extremes of pH.[14]) Apparent helical structure in P1/N3, P3/N1, and P3/N3 is possibly an artifact of deconvolution, a consequence of the relatively high average α helix propensity of P1 or N1,[40] or a consequence of side-chain hydrogen-bonding potential in P3 and N3 (Figure 1b). Deconvolution suggests that a large proportion of random coil (~7/10) and a small proportion of β sheet (~1/5) are present in P2/N2. Both P2/N3 and P3/N2 also have a large percentage of random coil (≥1/2). P1/N2 and P2/N1, by contrast, have a large percentage of β sheet (≥1/2); the molecules P2 and N2 have a high average propensity to form β sheets.[40] The high β turn content in the other films suggests protein-like β sheets: the higher the con-

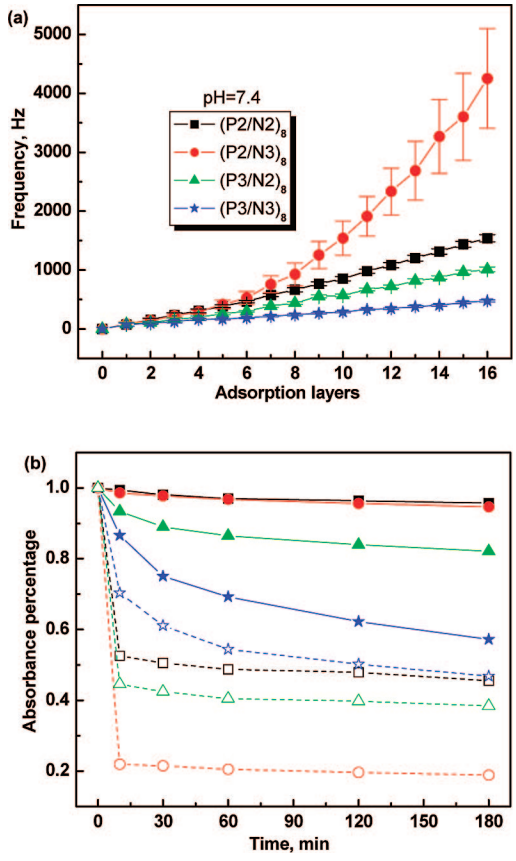

Figure 3. Assembly and disassembly of combinations of P2, N2, P3, and N3. (a) Assembly at pH 7.4 as monitored by QCM. The frequency increment is directly proportional to mass increment under the conditions of the experiment. (b) Disassembly at pH 4.0 (solid symbols) or pH 2.5 (open symbols) as monitored by UVS. Color coding of data points is the same in both panels. Film disassembly can be modeled as a first-order exponential decay process. The fitted time constants at pH 4.0 are 52 (P2/N2), 71 (P2/N3), 30 (P3/N2), and 36 min (P3/N3).

tent of β turns, the shorter and more protein-like the β strands.

The stability of the polypeptide multilayer nanofilms has been assessed by immersion into buffer at acidic pH.[16,17] Results obtained for P2, N2, P3, and N3, for example, are shown in Figure 3. The behavior of these peptides during nanofilm fabrication resembles the behavior of P1, N1, P2, and N2: it is context dependent (Figure 3a). Substantially more material is deposited for P2/N3 than for P2/N2 for a given number of layers. During disassembly at pH 4.0, P2/N2 and P2/N3 exhibit relatively little mass loss after 3 h (Figure 3b). P3/N2 and P3/N3, by contrast, show steady and substantial mass loss under the same conditions, the former retaining more mass than the latter. Film stability at mildly acidic pH is a direct reflection of the collective strength of noncovalent interactions between polymers and the film–substrate. Acidic conditions will induce the rupture of ionic bonds between oppositely charged peptides, even if the average pK_a of glutamic acid will vary with polymer structure, film architecture, and assembly conditions.[41,42] The behavior of P2/N2 and P2/N3 suggests that side-chain hydrogen-bonding and hydrophobic interactions, which are due to the structure of the side chains in these peptides (Figure 1b), will stabilize polyelectrolyte films under some conditions.[7,8,43] The hydrophobic surface is greater and the hydrogen-bonding potential is lower per peptide molecule in P3/N2 than in P3/N3. The nanofilm disassembly data in Figure 3b therefore suggest that satisfying hydrogen-bonding potential in the vicinity of neutral pH, which is known to be required in the hydrophobic core of proteins from crystal structure analysis, could destabilize a polypeptide film relative to hydrophobic interactions. A more certain conclusion

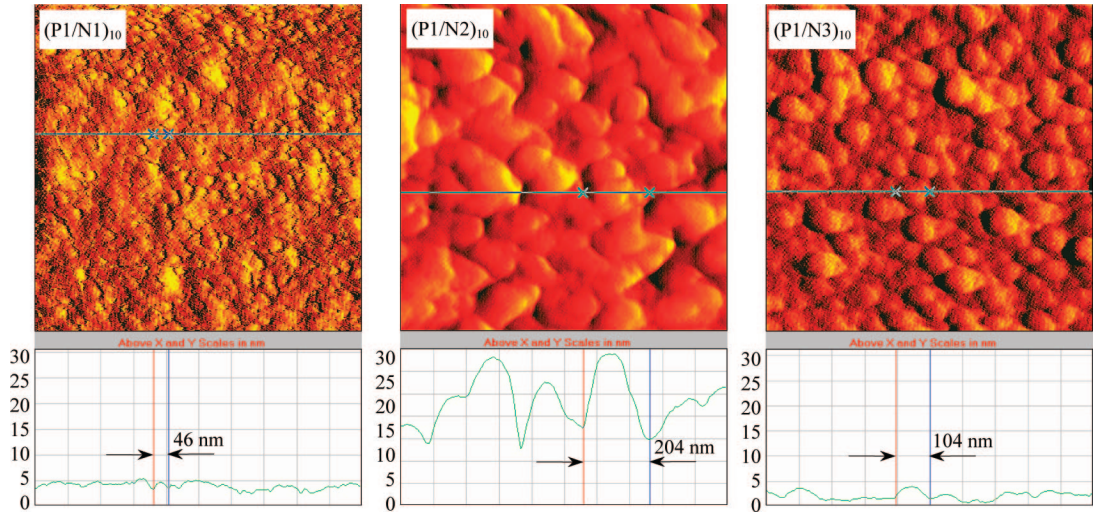

Figure 4. Surface morphology of P1 films as determined by AFM. Upper panels, height mode image; lower panels, profilometric section of the indicated location. The *z*-axis scale is 30 nm throughout. Note the large difference in granule size and surface roughness. These physical properties of a polypeptide multilayer film are context dependent; bulk properties are determined not by P1 *per se*, but by the interaction of P1 with the negatively charged peptide. Context dependence of surface morphology was found for the other peptide combinations as well (see Supporting Information).

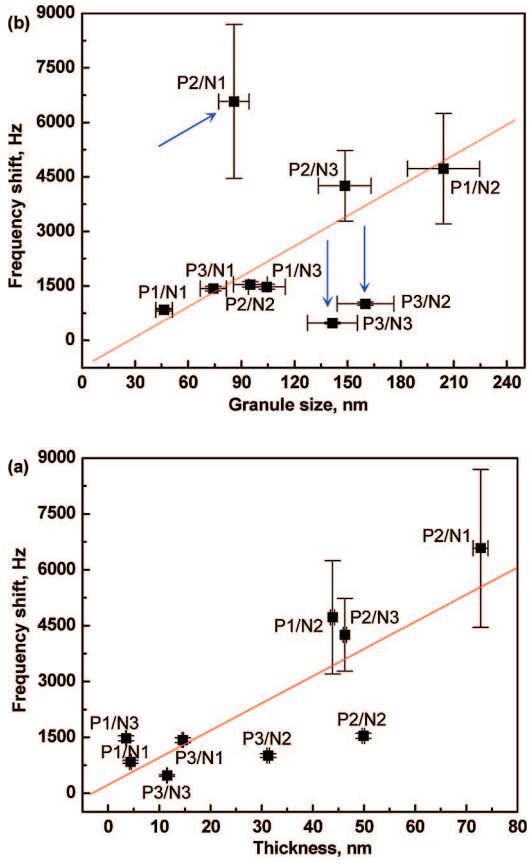

Figure 5. Relationship between frequency shift (film mass as determined by QCM), film thickness (as determined by ellipsometry), and granule size (surface roughness as determined by AFM). (a) Frequency shift *vs* thickness. The line, which represents the best-fit linear model to all data points, passes close by the origin; there is no change in frequency of a resonator unless peptide is adsorbed. Density varies between films by more than an order of magnitude, suggesting that direct translation of frequency shift into film thickness for different combinations of polyelectrolyte, though common in the scientific literature, is a dubious practice at best. (b) Frequency shift *vs* granule size. The error in frequency shift for P2/N1, P2/N2, and P2/N3 is the standard deviation of four independent samples. The error in ellipsometric thickness is the standard deviation of three randomly selected points on the same sample. The error in granule size is set to ±10% from analysis of AFM data. The line is a linear fit to all data points except those indicated by an arrow; it is a visual aid only.

is that the film properties of a given polypeptide are context dependent.

The pH dependence of film disassembly behavior has been characterized for different nanofilm architectures. The results show that behavior at pH 2.5 differs from that at pH 4.0. At pH 2.5, P3/N3 is the most stable film, P2/N3 is the least stable, and P2/N2 and P3/N2 are in between (Figure 3b). A relatively large percentage of glutamic acid side chains will be protonated at pH 2.5, weakening the electrostatic attraction between positive and negative peptides and increasing the inward migration of small counterions and charge repulsion between polycations. The effect of charge neutralization on P3/N3 will be less great than for the other

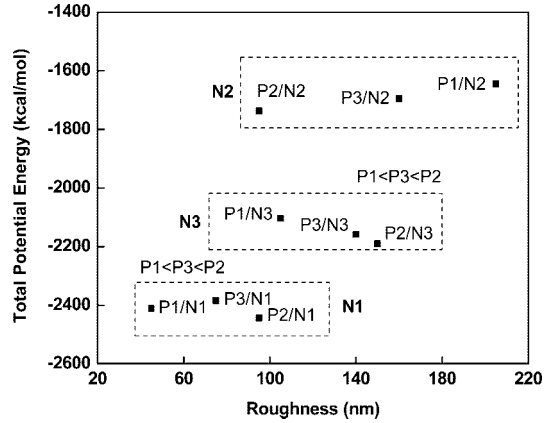

Figure 6. Calculated total potential energy in implicit solvent *versus* experimental surface roughness. With regard to surface roughness (*i.e.*, granule size), P1 < P3 < P2 in the N1 and N3 groups. With regard to total potential energy, N1 < N3 < N2. Potential energy is roughly correlated with film surface roughness.

films, because interactions between side-chain hydrophobic groups will tend to hold molecules together and polar side chains will contribute to the formation of hydrogen-bonding networks.

The reason why the order of stability of peptide systems is not the same at pH 2.5 as at pH 4.0 remains unclear. It seems likely, though, that any plausible explanation will have to involve both the probability of protonation of Glu side chains as a function of pH and the relative contribution of electrostatic interactions *versus* hydrophobic interactions and hydrogen bonds to nanofilm stability. In any case, the film disassembly data at acidic pH are consistent with a model in which Coulombic interactions dominate film stability, particularly at neutral pH, but hydrophobic interactions and hydrogen bonds are present and significant and in fact relatively important at acidic pH. This view is in accord with the predominant view of polyelectrolyte multilayer

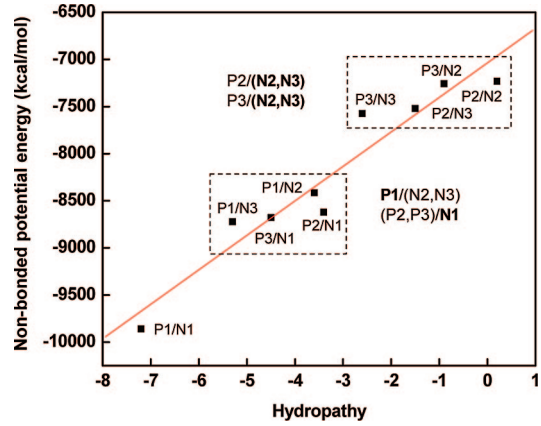

Figure 7. Calculated nonbonded potential energy in implicit solvent *versus* average hydropathy for the nine IPECs studied here. Average hydropathy per residue was calculated with data from ref 30. N2 has the highest average hydropathy. Generally, the greater the hydropathy, the greater the potential energy. P1/(N2,N3) is clustered with (P2,P3)/N1, and P2/(N2,N3) with (P2,P3)/N2.

film assembly,[1] but it seems contrary to the hypothesis that the hydrophobic effect is the dominant force in protein folding and stability.[27,28]

Basic features of the surface morphology of 20-layer polypeptide nanofilms built on silicon wafers have been determined by atomic force microscopy (AFM; Figure 4). "Granule size", defined as the diameter of a representative "grain-like" structure on the film surface, has been found to vary as P1/N1 < P2/N2 < P3/N3 by up to ~300% (Table 1). The high density of electrostatic interactions per unit mass in P1/N1 makes the film dense and smooth,[1] whereas the surface of P2/N2, which is stabilized internally by numerous hydrophobic interactions, is comparatively diffuse and rough. P3/N3 has a large granule size (142 nm), but the film is relatively smooth by profilometric analysis. Side-chain hydrogen bond donors and acceptors must form hydrogen bond networks in P3/N3, and charge interactions and hydrophobic interactions will be present. The need to satisfy hydrogen bond donors and acceptors and charge interactions in P3/N3 may induce structural irregularities in individual peptides and thus the entire film. Dehydration of hydrophobic groups during film drying in P3/N3 and P2/N2 will result in the "collapse" of structure, as in desolvation of hydrophobic core side chains in protein folding.[12,27] The overall secondary structure content of a polypeptide multilayer nanofilm is retained during drying and rewetting,[44] as in protein crystallization and lyophilization.

Film surface roughness (AFM) can be compared to mass of peptide deposited (QCM) and film thickness (ellipsometry). In Figure 5a, a linear fit to all data points distinguishes films of higher density (*e.g.*, P1/N3, 11.4 $g \cdot cm^{-3}$) from ones of lower density (*e.g.*, P2/N2, 0.84 $g \cdot cm^{-3}$ and P3/N2, 0.88 $g \cdot cm^{-3}$). The difference in extremes of density is huge. Figure 5b shows that nanofilm roughness tends to increase as mass deposited increases. Other researchers have suggested that supralinear film growth might arise from irregular polymer deposition, creating an increasingly rough surface and inducing interpenetration of layers.[45] The present results indicate that supralinear growth does not always correlate with surface roughness.

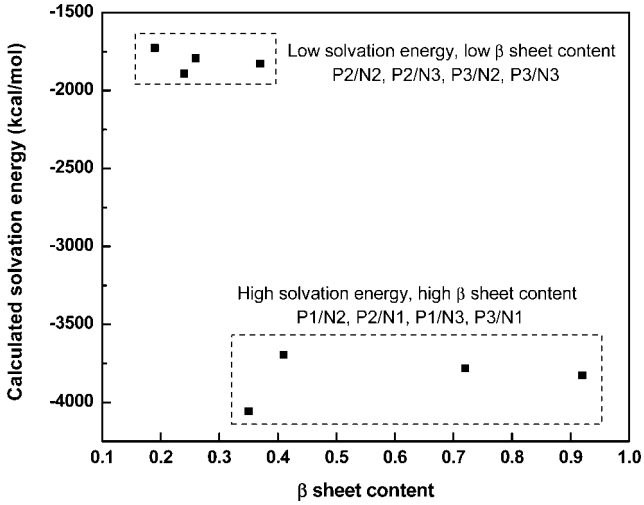

Figure 8. Relationship between calculated nonbonded potential energy of peptide pairs in implicit solvent and deconvoluted proportion of β sheet in the film. See Table 2. Note the clustering of P2/(N2,N3) with (P2,P3)/N2 and of P1/(N2,N3) with (P2,P3)/N1. The former IPECs have a net charge of 0, whereas the latter ones are only partially charge-neutralized.

Further analysis of the surface roughness data in Table 1 has revealed intriguing patterns. Experimental granule size follows the same order in peptide combinations involving N1 or N3: P1/N(1,3) < P3/N(1,3) < P2/N(1,3). Moreover, all film systems involving N1 have a smaller granule size than the corresponding system with N3. Furthermore, the order of granule size for combinations with P1 or P3 is the same as for N1 or N3: P(1,3)/N1 < P(1,3)/N3 < P(1,3)/N2. The cause of large granule size is apparently a difference in λ between peptides. The existence of patterns suggests the possibility that further study will reveal the underlying physical basis of the behavior. One way of gaining further understanding these peptide systems is to carry out MD simulations and to compare the results with experimental data.

Simulations. The behavior of IPECs corresponding to the combinations of peptide in the experimental studies described above has been analyzed in MD simulations. The approach is justified on the view that IPECs are a key analogue of polyelectrolyte multilayer films.[22] Simulations of larger aggregates of peptides were not feasible with the tools available for the work described here. All simulations were done in implicit solvent. In each case, the starting structure consisted of two oppositely charged peptides in a β sheet (Table 2) in order to base the simulations on the results of the experimental work (Table 1) and with classical bond angles in order to have a common reference state. The trajectory in each case was calculated for 1–2 ns, depending on the time required for the IPEC to reach equilibrium. Simulation results were compared with the experimental data presented above.

Figure 6 presents the calculated total potential energy of an IPEC in implicit solvent *versus* surface roughness of the corresponding polypeptide multilayer film for the various combinations of peptide (Table 1). IPEC energies clustered in three groups, determined apparently by the structure of the negative peptide because N1 < N3 < N2. The same order was found for granule size in systems of N1, N2, or N3 with P1 or P3. The polyanionic peptides may have a more significant effect on electrostatic potential than the polycationic peptides because the side-chain charges are closer to the polymer backbone in glutamate residues than in lysine residues.

The three groups of peptide systems with regard to electrostatic potential are also groups in terms of nanofilm surface roughness. The N1 group has the lowest

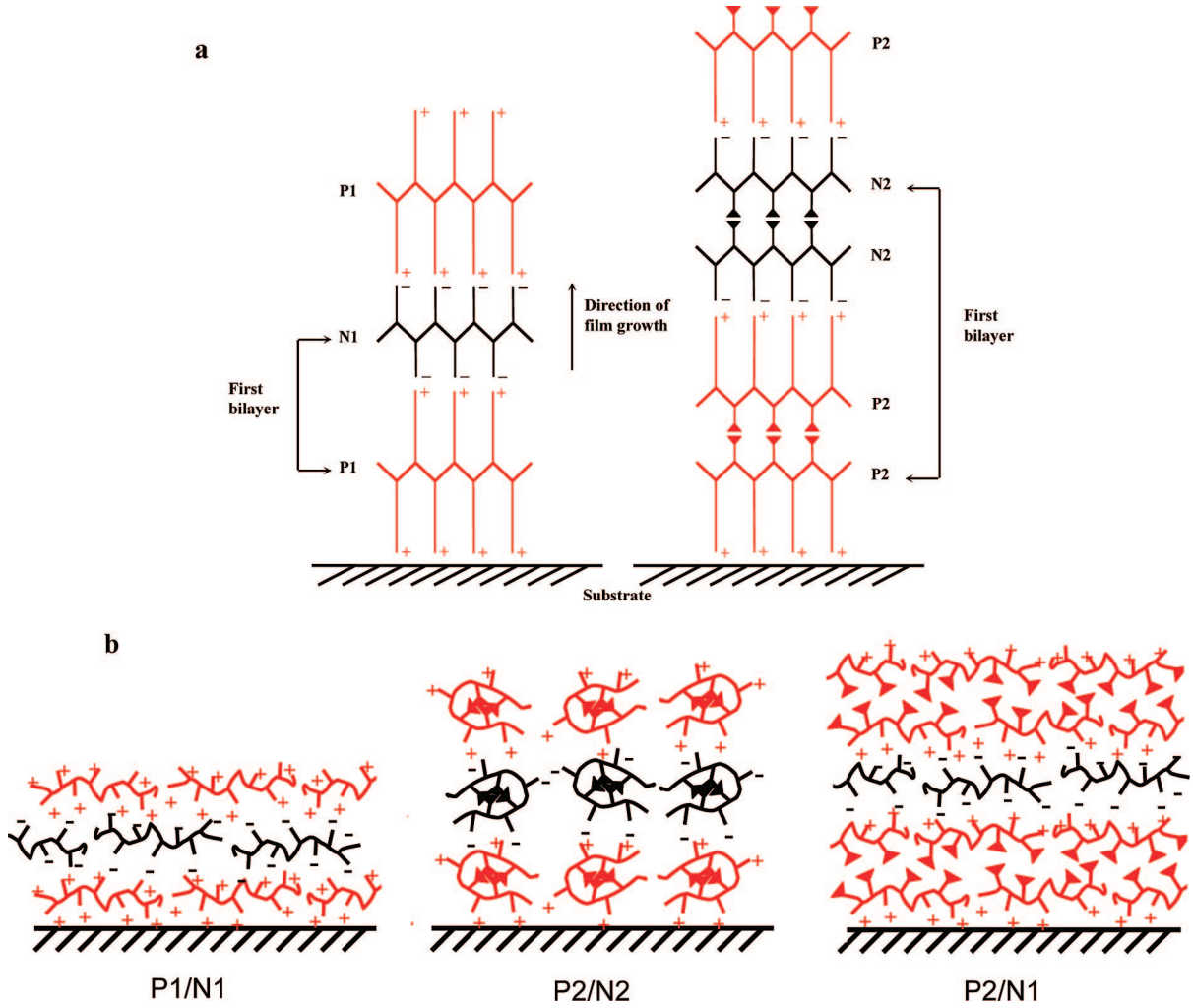

Figure 9. Film models based on experimental evidence presented here and in ref 46. (a) Highly schematic models of P1/N1 and P2/N2. Amino acid side chains are uniformly oriented in the plane of the page. Backbones are in a β sheet conformation (see Table 2). Each positive side-chain charge forms an ion pair with a negative side-chain charge. Hydrophobic side chains, indicated by triangles, interact not with charged side chains (energetically unfavorable) but with each other (energetically favorable). (b) More realistic models of P1/N1, P2/N2, and P2/N1. P1/N1 and P2/N2 grow linearly; P2/N1, exponentially. Again, the side chains are oriented vertically. This orientation is simpler to depict than horizontal side-chain orientation. The film situation must be more complex than the models suggest. See text for further discussion.

surface roughness; the N2 group, the highest. In the N1 and N3 groups, nanofilm surface roughness follows the same pattern as calculated IPEC total potential energy: P1/N(1,3) < P3/N(1,3) < P2/N(1,3). The data suggest that peptide combinations with a high charge density and strong interaction energy will tend to have a low surface roughness, and *vice versa*. The results also support the idea that the greater the similarity of peptide structures in a peptide pair, the higher the energy of interaction in an IPEC, especially when hydrophobic interactions are involved, and the lower the surface roughness of the corresponding film.

Calculated nonbonded potential energies of IPECs correlate with average per-residue hydropathy values (Figure 7). An experimentally determined quantity, hydropathy measures the tendency of a compound to avoid partitioning into water from a less polar solvent. Hydropathy is calculated from the transfer free energy of a compound between an organic phase and water. Hydrophobic side chains have a higher hydropathy than hydrophilic side chains. The data in Figure 7 show that the higher the charge density of a polyelectrolyte, the greater the electrostatic contribution of the IPEC to potential energy, the lower the potential energy of the peptide complex, and the lower the hydropathy.

Comparison of computational results and experimental data has revealed that the calculated solvation energy of an IPEC correlates with the deconvoluted percentage of β sheet in the corresponding multilayer film (Figure 8). The larger the solvation energy, the more probable the formation of β sheet in the film. The relationship suggests that the propensity of a peptide to form secondary structure in a multilayer film will not be a function of amino acid sequence alone[43] but also of the structure of its assembly partner.

Models. Idealized structural models of P1/N1 and P2/N2 are shown in Figure 9a. Individual molecules of P1 and N1 have the maximum possible value of λ at neutral pH: all side chains are charged;[24] these polymers are highly soluble. Experimental data support the view that the ratio of deposition of P1 to N1 in successive film layers is 1:1,[46] which is consistent with the view that approximately one "layer" of molecules is deposited per deposition cycle. Charge repulsion will be high between molecules within a single film layer. Each layer will be comparatively thin because the contour length of the polymers and the ionic strength are low (refs 1, 10, and 13; Table 1). In the copolypeptides P2 and N2, by contrast, hydrophobic residues alternate with charged ones at neutral pH. The nonpolar side chains will strongly influence peptide structure and solubility. P2 can form β sheet-containing fibrils in aqueous solution.[47,48] Experimental evidence indicates that the mass ratio of P2 (or N2) deposition to that of N1 (or P1) is close to 2 (ref 46; Supporting Information). Stacking of layers will be stabilized by hydrophobic interactions between valine residues.[47]

More realistic nanofilm models, of P1/N1, P2/N2, and P2/N1, are shown in Figure 9b. Highly charged P1 and N1 can readily form favorable charge pairs between layers. These polymers are likely to adopt a relatively extended conformation because intramolecular charge repulsion is high and degree of polymerization is low. β sheet structure is present.[14,44] The lesser charged polymers P2 and N2 are more likely to show intrachain clustering due to the large number of hydrophobic side chains. "Collapse" of peptide structure on itself, if it occurs, could hinder formation of favorable charge pairs between layers. P2 and N2 could also be deposited in a single layer per adsorption step, leading to less β sheet formation, more charge repulsion within each plane, and a less highly networked film. In the case of P2/N1 (or P1/N2), there will be less conformation-based hindrance of formation of ordered structure, if any at all, because the overall density of charged groups in the film will be higher than in P2/N2. These charged groups will increase the tendency of the peptides to adopt an extended conformation, as in P1/N1. Layer stacking is more probable at each adsorption step involving P2 or N2 than P1 or N1.[46]

METHODS

Peptides. Six 32mer peptides, designated P1, N1, P2, N2, P3, and N3 (Figure 1a), were designed to test the role of electrostatic interactions, hydrophobic interactions, and hydrogen-bonding potential in LBL.[23] Details of the chemical structure of the amino acid constituents of these peptides—lysine (Lys), glutamic acid (Glu), valine (Val), serine (Ser), glutamine (Gln), and tyrosine (Tyr)—are depicted in Figure 1b. The polypeptides were synthesized by standard F-moc solid-phase synthesis, purified, characterized by mass spectrometry and high-performance liquid chromatography, and lyophilized prior to incorporation into multilayer nanofilms. Some sequence heterogeneity was tolerated. Most polyelectrolyte multilayer film studies involve highly polydisperse preparations of polymers. Earlier work from our laboratory has shown that the same preparations of peptides display behavior that can be predicted on the basis of amino acid sequence.[46]

Solutions. All polypeptide multilayer nanofilms were fabricated by LBL (Figure 1c). A schematic of the product of polypeptide LBL is shown in Figure 1d.[1] For nanofilm fabrication, lyophilized peptides were dissolved in 10 mM tris(hydroxymethyl)aminomethane buffer, 10 mM NaCl, pH 7.4, to a final concentration of 2 mg/mL. The peptide adsorption time was 15 min per adsorption step (*i.e.*, per "layer"). Disassembly experiments were done by immersing nanofilms in 10 mM acetate buffer, 10 mM NaCl, pH 4.0, or 10 mM glycine buffer, 10 mM NaCl, pH 2.5. All nanofilms were rinsed three times with deionized water and dried with a gentle stream of nitrogen gas after each assembly or disassembly step.

Instruments. A quartz crystal microbalance (Agilent 53131A, 225 MHz universal counter, Agilent Technologies, Santa Clara, CA) was used to monitor the sequential assembly of the films on silver-coated resonators with a nominal frequency of 9 MHz and a surface area of 0.16 cm^2 (Sanwa Tsusho Co., Ltd., Tokyo, Japan). Quartz microscope slides for ultraviolet spectroscopy (UV-1650 PC UV–vis spectrophotometer, Shimadzu Corp., Kyoto, Japan) and circular dichroism spectrometry (J-810 spectropolarimeter, Jasco Corp., Tokyo, Japan) were from Electron Microscopy Sciences (Hatfield, PA). The step size for CD experiments was 0.1 nm, and the bandwidth was 1 nm. The thickness and surface morphology of nanofilms prepared on silicon wafers were characterized by ellipsometry (SE 850 ellipsometer, Sentech Instruments GmbH, Berlin, Germany) and atomic force microscopy (Q-Scope 250 AFM, Quesant Instrument Corp., Santa Cruz, CA), respectively. Silicon wafers (N/Phos ⟨100⟩, resistivity 1–10 Ω · cm, thickness 375–425 μm, diameter 100 ± 0.5 mm, bare silicon) were from Silicone Technology Corp. (Newport News, VA). A very thin layer of naturally grown SiO_2 was present on the Si surface. Details of substrate cleaning procedures, instrument settings, and deconvolution of CD spectra can be found in refs 13, 14, 16, and 49.

Simulations. Twenty-six qualitatively different MD simulations of IPECs in implicit solvent were done: P1−N1 with parallel strands (P1−N1_P); P1−N1 with antiparallel strands (P1−N1_A); P2−N2 with charged side chains on same side of the β sheet (P2−N2_PS, P2−N2_AS); P2−N2 with charged side chains on opposite sides of the β sheet (P2−N2_PO, P2−N2_AO); and so on, including P3−N3_PO, P3−N3_AO, P3−N3_PS, P3−N3_AS, P1−N2_P, P1−N2_A, P2−N1_P, P2−N1_A, P1−N3_P, P1−N3_A, P3−N1_P, P3−N1_A, P2−N3_PO, P2−N3_AO, P2−N3_PS, P2−N3_AS, P3−N2_PO, P3−N2_AO, P3−N2_PS, and P3−N2_AS. The starting structure was a β sheet with classical bond angles in each case. 32mer peptide models were built with the Biopolymer module of Insight II (Accelrys, San Diego, CA) to represent the peptides studied in the experiments described here.[23] All simulations were run with the Amber 8 simulation package[50] and the ff99 force field.[51] Each peptide IPEC configuration was simulated in implicit solvent. The GB solvation model (igb = 5) was used,[52] the salt concentration was 15 mM, and the pH was 7.4. At this pH, glutamic acid is negatively charged and lysine is positively charged with high probability. The protonation state of Glu and Lys side chains therefore was fixed in the ionized state. Each IPEC system was energy minimized for 1000 cycles prior to MD simulation, and each residue was constrained to its original position by a harmonic potential with a force constant of 5.0 kcal · mol^{-1} · $Å^{-2}$. The system was heated from 240 to 300 K in 10 ps and weakly coupled to a Berendsen temperature bath at 300 K for 1 ns with a time constant of 2 ps.[53] Lengths of bonds involving a hydrogen atom were constrained with the SHAKE algo-

rithm.[54] The time step for MD was 2 fs. Each MD trajectory was sampled every 1 ps for further analysis with DeCipher (Accelrys). Attainment of equilibrium was ascertained in each case by analysis of the time course of potential energy. Each qualitatively different simulation was repeated at least once. In all cases, the outcome of the repeated simulation was essentially the same as the original.

Acknowledgment. We thank Robert Woody for helpful comments on deconvolution of CD spectra and Dr. Bingyun Li for discussions. This work was supported by a developmental project allocation on the Xeon Linux Supercluster at the National Center for Supercomputing Applications (MCB050011), an enhancement grant from the Louisiana Board of Regents (LEQSF(2003–04)-ENH-TR-42), a seed grant from the Center for Entrepreneurship and Information Technology, a project grant from Artificial Cell Technologies, Inc., an enhancement grant from the Louisiana Space Consortium (Louisiana NASA EPSCoR, project R127172), the 2002 Capital Outlay Act 23 of the State of Louisiana (Governor's Biotechnology Initiative), and a Nanoscale Exploratory Research award (DMI-0403882) and an Instrumentation for Materials Research award (DMR-0414903) from the National Science Foundation.

Supporting Information Available: Proof of exponential film buildup in the case of P2/N1; CD spectra of P2/N2 and P3/N2 at different stages of film buildup and at different time points during disassembly at pH 2.5; comparison of film buildup of P2/N1 and P1/N2; surface morphology of P2 and P3 films as determined by AFM. This material is available free of charge *via* the Internet at http://pubs.acs.org.

REFERENCES AND NOTES

1 Decher, G. Fuzzy Nanoassemblies: Toward Layered Polymeric Multicomposites. *Science* **1997**, *277*, 1232–1237.
2 Bertrand, P.; Jonas, A.; Laschewsky, A.; Legras, R. Ultrathin Polymer Coatings by Complexation of Polyelectrolytes at Interfaces: Suitable Materials, Structure and Properties. *Macromol. Rapid Commun.* **2000**, *21*, 319–348.
3 Lvov, Y., Möhwald, H., Eds. *Protein Architecture: Interfacing Molecular Assemblies and Immobilization Biotechnology*; Marcel Dekker: New York, 2000.
4 Tripathy, S. K., Kumar, J., Nalwa, H. S., Eds. *Handbook of Polyelectrolytes and Their Applications. Vol. 1. Polyelectrolyte-based Multilayers, Self-assemblies and Nanostructures*; American Scientific: Stevenson Ranch, CA, 2002.
5 Haynie, D. T.; Zhang, L.; Rudra, J. S.; Zhao, W.; Zhong, Y.; Palath, N. Polypeptide Multilayer Films. *Biomacromolecules* **2005**, *6*, 2895–2913.
6 Iler, R. K. Multilayers of Colloidal Particles. *J. Colloid Interface Sci.* **1966**, *21*, 569–594.
7 Kotov, N. A. Layer-by-Layer Self-Assembly: The Contribution of Hydrophobic Interactions. *Nanostruct. Mater.* **1999**, *2*, 789–796.
8 Hammond, P. T. Recent Explorations in Electrostatic Multilayer Thin Film Assembly. *Curr. Opin. Colloid Interface Sci.* **2000**, *4*, 430–442.
9 Hammond, P. T. Form and Function in Multilayer Assembly: New Applications at the Nanoscale. *Adv. Mater.* **2004**, *16*, 1271–1293.
10 Haynie, D. T. Physics of Polypeptide Multilayer Films. *J. Biomed. Mater. Res. B Appl. Biomater.* **2006**, *78B*, 243–252.
11 Creighton, T. E. *Proteins: Structures and Molecular Properties*, 2nd ed.; Freeman: New York, 1993.
12 Finkelstein, A. V.; Ptitsyn, O. B. *Protein Physics: A Course of Lectures*; Academic: Amsterdam, 2002.
13 Zhang, L.; Li, B.; Zhi, Z.-l.; Haynie, D. T. Perturbation of Nano-Scale Structure of Polypeptide Multilayer Thin Films. *Langmuir* **2005**, *21*, 5439–5445.
14 Zhi, Z.-l.; Haynie, D. T. Direct Evidence of Controlled Structure Reorganization in a Nanoorganized Polypeptide Multilayer Thin Film. *Macromolecules* **2004**, *37*, 8668–8675.
15 Li, B.; Rozas, J.; Haynie, D. T. Structural Stability of Polypeptide Nanofilms under Extreme Conditions. *Biotechnol. Prog.* **2006**, *22*, 111–117.
16 Zhong, Y.; Li, B.; Haynie, D. T. pH Adjustment Enables Exquisite Control over Fabrication of Designed Peptide Multilayer Nanofilms. *Biotechnol. Prog.* **2006**, *22*, 126–132.
17 Li, B.; Haynie, D. T. Multilayer Biomimetics: Reversible Covalent Stabilization of a Nanostructured Biofilm. *Biomacromolecules* **2005**, *5*, 1667–1670.
18 Li, B.; Haynie, D. T.; Palath, N.; Janisch, D. Nano-Scale Biomimetics: Fabrication and Optization of Stability of Peptide-Based Multilayer Thin Films. *J. Nanosci. Nanotechnol.* **2005**, *5*, 2042–2049.
19 Zhong, Y.; Li, B.; Haynie, D. T. Control of Stability of Polypeptide Multilayer Nanofilms by Quantitative Control of Disulfide Bond Formation. *Nanotechnology* **2006**, *17*, 5726–5734.
20 Haynie, D. T.; Palath, N.; Liu, Y.; Li, B.; Pargaonkar, N. Biomimetic Nanotechnology: Inherent Reversible Stabilization of Polypeptide Microcapsules. *Langmuir* **2005**, *21*, 1136–1138.
21 Zhao, W.; Zheng, B.; Haynie, D. T. A Molecular Dynamics Study of the Physical Basis of Stability of Polypeptide Multilayer Nanofilms. *Langmuir* **2006**, *22*, 6668–6675.
22 Kabanov, V. Fundamentals of Polyelectrolyte Complexes in Solution and the Bulk. In *Multilayer Thin Films: Sequential Assembly of Nanocomposite Materials*; Decher, G., Schlenoff, J. B., Eds.; Wiley-VCH: Weinheim, 2003; pp 47–86.
23 Haynie, D. T.; Zhang, L.; Zhao, W. Polypeptide Multilayer Films: Experiments, Simulations, Implications. *Polym. Mater. Sci. Eng.* **2005**, *94*, 95–97.
24 Doty, P.; Wada, A.; Yang, J. T.; Blout, E. R. Polypeptides VIII. Molecular Configurations of Poly-L-Glutamic Acid in Water-Dioxane Solution. *J. Polym. Sci.* **1957**, *23*, 851–861.
25 Kyte, J.; Doolittle, R. F. A Simple Method for Displaying the Hydropathic Character of a Protein. *J. Mol. Biol.* **1982**, *157*, 105–132.
26 Zheng, B.; Haynie, D. T.; Zhong, H.; Sabnis, K.; Surpuriya, V.; Pargaonkar, N.; Sharma, G.; Vistakula, K. Design of Peptides for Thin Films, Coatings, and Microcapsules for Applications in Biotechnology. *J. Biomater. Sci. Polym. Edn.* **2005**, *16*, 285–300.
27 Dill, K. A. Dominant Forces in Protein Folding. *Biochemistry* **1990**, *29*, 7133–7155.
28 Fersht, A. R. *Structure and Mechanism in Protein Science*; Freeman: New York, 1999.
29 Yang, J. T.; Wu, C.-s.; Martinez, H. M. Calculation of Protein Conformation from Circular Dichroism. *Methods Enzymol.* **1986**, *130*, 208–269.
30 Johnson, W. C., Jr. Secondary Structure of Proteins through Circular Dichroism Spectroscopy. *Annu. Rev. Biophys. Biophys. Chem.* **1988**, *17*, 145–166.
31 Sreerama, N.; Woody, R. W. Circular Dichroism of Peptides and Proteins. In *Circular Dichroism: Principles and Applications*, 2nd ed.; Berova, N., Nakanishi, K., Woody, R. W., Eds.; Wiley: New York, 2000, pp 601–620.
32 Stevens, L.; Townend, R.; Timasheff, S. N.; Fasman, G. D.; Potter, J. The Circular Dichroism of Polypeptide Films. *Biochemistry* **1968**, *7*, 3717–3720.
33 Fasman, G. D.; Hoving, H.; Timasheff, S. N. Circular Dichroism of Polypeptide and Protein Conformations. Film studies. *Biochemistry* **1970**, *9*, 3316–3324.
34 Cerpa, R.; Cohen, F. E.; Kuntz, I. D. Conformational Switching in Designed Peptides: The Helix/Sheet Transition. *Folding Des.* **1996**, *1*, 91–101.
35 Minor, D. L., Jr.; Kim, P. S. Context-Dependent Secondary Structure Formation of a Designed Protein Sequence. *Nature* **1996**, *380*, 730–734.
36 Deechongkit, S.; Nguyen, H.; Powers, E. T.; Dawson, P. E.; Gruebele, M.; Kelly, J. W. Context-Dependent Contributions of Backbone Hydrogen Bonding to β-Sheet Folding Energetics. *Nature* **2004**, *430*, 101–105.

37 Balkundi, S. Insight into Polypeptide Layer-by-Layer Assembly Using the Models Poly-L-Lysine and Poly-L-Glutamic Acid. M.S. thesis, LA Tech University, 2004.
38 Manavalan, P.; Johnson, W. C., Jr. Sensitivity of Circular Dichroism to Protein Tertiary Structure Slass. *Nature* **1983**, *305*, 831–832.
39 Sreerama, N.; Woody, R. W. Estimation of Protein Secondary Structure from CD Spectra: Comparison of CONTIN, SELCON and CDSSTR Methods with an Expanded Reference Set. *Anal. Biochem.* **2000**, *282*, 252–260.
40 Chou, P. Y.; Fasman, G. D. Conformational Parameters for Amino Acids in Helical, Beta-Sheet, and Random Coil Regions Calculated from Proteins. *Biochemistry* **1974**, *13*, 211–222.
41 Mendelsohn, J. D.; Barrett, C. J.; Chan, V. V.; Pal, A. J.; Mayes, A. M.; Rubner, M. F. Fabrication of Microporous Thin Films from Polyelectrolyte Multilayers. *Langmuir* **2000**, *16*, 5017–5023.
42 Xie, A. F.; Granick, S. Weak Versus Strong: A Weak Polyacid Embedded within a Multilayer of Strong Polyelectrolytes. *J. Am. Chem. Soc.* **2001**, *123*, 3175–3176.
43 Laschewsky, A.; Wischerhoff, E. Polyelectrolyte Multilayer Assemblies Containing Nonlinear Optical Dyes. *Macromolecules* **1997**, *30*, 8304–8309.
44 Zhang, L.; Haynie, D. T. Comparative Analysis of Wet and Dry Polypeptide Multilayer Films. *Biomacromolecules* **2007**, *8*, 2033–2037.
45 Sukhishvili, S.; Granick, S. Layered, Erasable Polymer Multilayers Formed by Hydrogen-Bonded Sequential Self-Assembly. *J. Am. Chem. Soc.* **2000**, *122*, 9550–9551.
46 Haynie, D. T.; Zhang, L.; Zhao, W.; Smith, J. M. Quantal Self-Assembly of Polymer Layers in Polypeptide Multilayer Films. *Biomacromolecules* **2006**, *7*, 2264–2268.
47 Brack, A.; Orgel, L. E. β Structures of Alternating Polypeptides and their Possible Prebiotic Significance. *Nature* **1975**, *256*, 383–387.
48 Lamm, M. S.; Rajagopal, K.; Schneider, J. P.; Pochan, D. Laminated Morphology of Nontwisting Beta-Sheet Fibrils Constructed via Peptide Self-Assembly. J. *J. Am. Chem. Soc.* **2005**, *127*, 16692–16700.
49 Haynie, D. T.; Balkundi, S.; Palath, N.; Chakravarthula, K.; Dave, K. Polypeptide Multilayer Films: Role of Molecular Structure and Charge. *Langmuir* **2004**, *20*, 4540–4547.
50 Case, D. A.; Darden, T. A.; Cheatham, T. E., III; Simmerling, C. L.; Wang, J.; Duke, R. E.; Luo, R.; Merz, K. M.; Wang, B.; Pearlman, D. A.; *Amber 8*; University of Clifornia, San Francisco, 2004.
51 Wang, J.; Cieplak, P.; Kollman, P. A. How Well Does a Restrained Electrostatic Potential (RESP) Model Perform in Calculating Conformational Energies of Organic and Biological Molecules. *J. Comput. Chem.* **2000**, *21*, 1049–1074.
52 Onufriev, A.; Bashford, D.; Case, D. A. Effective Born Radii in the Generalized Born Approximation: The importance of Being Perfect. *Proteins* **2004**, *55*, 383–394.
53 Berendsen, H. J. C.; Postma, J. P. M.; van Gunsteren, W. F.; DiNola, A.; Haak, J. R. Molecular Dynamics with Coupling to an External Bath. *J. Chem. Phys.* **1984**, *81*, 3684–3690.
54 Rychaert, J. P.; Ciccotti, G.; Berendsen, H. J. C. Numerical Integration of the Cartesian Equations of Dynamics of *n*-Alkanes. *J. Comput. Phys.* **1977**, *23*, 327–341.